Structural model of phospholipid-reconstituted human transferrin receptor derived by electron microscopy

Hendrik Fuchs[1†], Uwe Lücken[2‡], Rudolf Tauber[1†], Andreas Engel[3] and Reinhard Geßner[1*]

Background: The transferrin receptor (TfR) regulates the cellular uptake of serum iron. Although the TfR serves as a model system for endocytosis receptors, neither crystal structure analysis nor electron microscopy has yet revealed the molecular dimensions of the TfR. To derive the first molecular model, we analyzed purified, lipid-reconstituted human TfR by high-resolution electron microscopy.

Results: A structural model of phospholipid-reconstituted TfR was derived from 72 cryo-electron microscopic images. The TfR dimer consists of a large extracellular globular domain ($6.4 \times 7.5 \times 10.5$ nm) separated from the membrane by a thin molecular stalk (2.9 nm). A comparative protein sequence analysis suggests that the stalk corresponds to amino acid residues 89–126. Under phospholipid-reconstitution conditions, the human TfR not only integrates into vesicles, but also forms rosette-like structures called proteoparticles. Scanning transmission electron microscopy revealed an overall diameter of 31.5 nm and a molecular mass of 1669 ± 26 kDa for the proteoparticles, corresponding to nine TfR dimers. The average mass of a single receptor dimer was determined as being 186 ± 4 kDa.

Conclusions: Proteoparticles resemble TfR exosomes that are expelled by sheep reticulocytes upon maturation. The structure of proteoparticles *in vitro* is thus interpreted as being the result of the TfR's strong self-association potential, which might facilitate the endosomal sequestration of the TfR away from other membrane proteins and its subsequent return to the cell surface within tubular structures. The stalk is assumed to facilitate the tight packing of receptor molecules in coated pits and recycling tubuli.

Addresses: [1]Institut für Laboratoriumsmedizin und Pathobiochemie, Charité, Campus Virchow-Klinikum, Augustenburger Platz 1, D-13353 Berlin, Germany, [2]Fritz-Haber-Institut der Max-Planck-Gesellschaft, Faradayweg, D-14195 Berlin, Germany and [3]Maurice E. Müller Institute for Electron Microscopy at the Biocenter, University of Basel, Klingelbergstraße 70, CH-4056 Basel, Switzerland.

Present addresses: [†]Institut für Klinische Chemie und Pathobiochemie, Universitätsklinikum Benjamin Franklin, Freie Universität Berlin, Hindenburgdamm 30, D-12200 Berlin, Germany and [‡]Philips Electron Optics, Achtseweg Noord, NL-5600 MD, Eindhoven, The Netherlands.

*Corresponding author.
E-mail: gessner@charite.de

Key words: cryo-electron microscopy, mass analysis, membrane protein, molecular stalk, STEM

Received: **15 June 1998**
Revisions requested: **3 July 1998**
Revisions received: **22 July 1998**
Accepted: **27 July 1998**

Structure 15 October 1998, **6**:1235–1243
http://biomednet.com/elecref/0969212600601235

Introduction

In vertebrates the transferrin receptor (TfR) mediates cellular iron uptake upon binding and endocytosis of the serum iron transport protein transferrin. Within the acidic microenvironment of early endosomes, iron ions dissociate from transferrin and are transported into the cytoplasm. The TfR–apotransferrin complex is separated from other endocytosed membrane proteins and then recycled back to the cell surface via a tubular network [1–3].

The expression of TfR is tightly linked to the cellular free iron concentration by a translational regulatory mechanism [4,5]. In most somatic cells, the TfR is degraded slowly with a half life of 14–16 h [6–8]; an additional fast degradation is found in maturing reticulocytes, which either expel excess TfR in the form of exosomes [9] or release the extracellular region by proteolytic cleavage [10].

The human TfR is a homodimeric membrane protein of about 190 kDa [10,11]. The cytoplasmic region (residues 1–67) is phosphorylated [12] at Ser24 and palmitoylated next to the transmembrane domain [13] (residues 68–88) at Cys62 and Cys67. The large extracellular regions of the TfR (residues 89–760) are covalently linked by two disulfide bridges [14] (Cys89 and Cys98) and carry one O-linked [15,16] and three N-linked glycans [17].

Whereas the primary structure of the human TfR [18,19], its posttranslational modifications and its intracellular trafficking (as reviewed in [20]) have been known for many years, its three-dimensional structure has not yet been published. The only successful crystallization reported [21] was performed with a tryptic fragment comprising most of the extracellular part of the receptor (122–760). Structure determination proved to be extremely difficult, however, and the work is expected to be completed soon (CM Lawrence & SC Harrison, personal communication). Although purified TfR can be reconstituted into phospholipid vesicles [22–24], no structural model has been derived from electron microscopy (EM) data so far.

Upon reconstituting the purified human TfR into phospholipid vesicles, we had previously observed the formation of three distinct TfR superstructures: vesicles with membrane-integrated TfRs, tubular structures and proteoparticles [24]. Proteoparticles appeared as rosette-like structures in standard negative-stain images and exhibited a molecular mass exceeding 1000 kDa in gel filtration experiments [24]. In order to derive a structural model for the TFR dimer and to elucidate the exact geometry of TfR proteoparticles, we applied scanning transmission electron microscopy (STEM) and cryoelectron microscopy (cryo-EM) to purified and to phospholipid-reconstituted human TfR. We were able to show that the TfR consists of a large globular domain ($6.4 \times 7.5 \times 10.5$ nm) separated from the membrane by a 2.9 nm molecular stalk. Additionally, we showed that the receptor forms specific proteoparticles containing, on average, nine receptor dimers.

Results and discussion

STEM analysis of proteoparticles

Proteoparticles do not only form when solubilized receptor dimers are reconstituted into phospholipid bilayers; they also appear to be the predominant conformation of purified TfR in the absence of detergent [23]. Upon adsorption of detergent-free human TfR onto ultrathin carbon films, rosette-like structures of uniform size and much smaller particles that appear to represent isolated receptor dimers can be visualized by STEM (Figure 1a). A close examination of the micrographs at higher resolution reveals that the rosette-like structures are formed by a central density surrounded by eight to ten compact particles of similar size and shape to the isolated small particles (Figure 1b–d). The size of the proteoparticles was determined to be 31.5 ± 2.9 nm by analyzing 62 different proteoparticles, as is described in the materials and methods section.

Figure 1

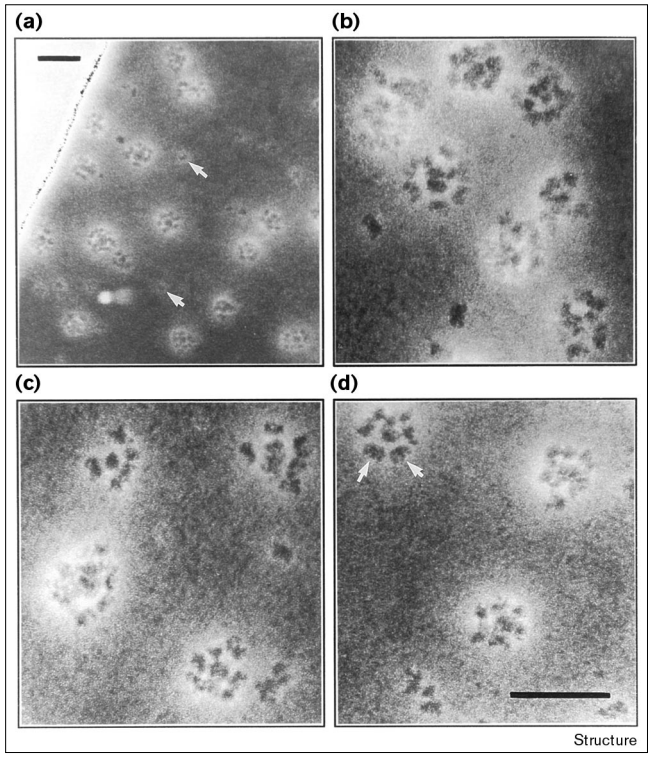

STEM elastic darkfield signal of TfR proteoparticles. Detergent-free human TfR sample was adsorbed to carbon-coated copper grids. The grids were intensively washed with distilled water, negatively stained with uranyl formate and air-dried. **(a)** A typical section displaying many TfR proteoparticles and a few isolated receptor dimers (indicated by arrows). **(b–d)** Similar sections at higher magnification. The proteoparticles consist of about nine receptor dimers, of which some appear almost bilobular with a small cleft at the outer face (arrows in d). Scale bars: 50 nm.

STEM offers a unique opportunity to determine the mass of a single macromolecule by measuring the electrons it scatters [25]. The accuracy of this method can be enhanced by recording a large number of objects and calculating their mass distribution. Such a mass distribution of 587 randomly chosen objects from our images is displayed in Figure 2a. Partitioning the x axis into intervals of 112 kDa, a sharp peak is found at the left margin and a broad peak at about 1700 kDa. When choosing smaller intervals (Figure 2b), the left peak appears to be highly symmetric and can be approximated by a Gaussian curve within the selected 0–290 kDa mass range ($r = 0.977$). The curve has a maximum at 185.9 kDa, with a standard error of 4.2 kDa (n = 121). This molecular mass corresponds perfectly with the published mass range for the human TfR dimer of 180–190 kDa [11,26–28]. This experimentally derived number was used to interpret the broad peak displayed in Figure 2a. A Gaussian curve fit ($r = 0.948$) of 427 particles within the 843–3202 kDa mass range revealed an average proteoparticle mass of 1669 ± 26 kDa. This value corresponds to nine TfR dimers. The large standard deviation ($\sigma = 533$ kDa) indicates a nonstoichiometric particle composition covering a range of 9 ± 3 receptor dimers. The mass analysis gives a more accurate estimate of the average number of receptor dimers within the proteoparticles than the visual inspection of the images displayed in Figure 1.

Solution structure of the human TfR in amorphous ice

Most EM techniques rely on the adsorption of the analyzed macromolecules to the surface of the carbon film and therefore carry the risk of altering the conformation of the macromolecules. In addition, staining procedures can induce distortions and change the apparent shape of the sample. In contrast, cryo-EM is superior to other EM techniques as it enables the visualization of a thin section of a shock-frozen sample without artificially induced conformational distortions [29,30]. Thus, the human TfR was reconstituted into phospholipid vesicles and visualized by cryo-EM (Figure 3). Whereas some large phospholipid vesicles are bilamellar or multilamellar (open arrow in the

top panel, Figure 3), all vesicles with membrane-integrated TfR are unilamellar and smaller in size (arrowheads in bottom panels). The few scattered membrane fragments also contain TfR molecules integrated from both sides (arrowheads in top panels). Some small vesicles seem to be in the process of integrating TfR from groups of proteoparticles (thick arrows). Isolated proteoparticles can be found randomly distributed in all micrographs (thin arrows).

Compared to those seen in the STEM analysis, the proteoparticles in amorphous ice exhibit a similar shape but a somewhat smaller overall diameter of 28.1 ± 2.4 nm (Figure 3). Assuming a near spherical shape of the proteoparticles, this small difference can easily be explained by the molecular distortion induced in the STEM analysis by the adsorption to the carbon film. A concurrent dynamic light-scattering analysis of the same batch of TfR proteoparticles in aqueous solution revealed a hydrodynamic diameter of 31.0 ± 2.6 nm (J Schüler, Y Georgalis, HF, P Umbach, W Saenger & RG, unpublished results). Thus, proteoparticles formed upon phospholipid reconstitution of completely solubilized human TfR and those present in detergent-free receptor solution are approximately the same size. Moreover, TfR proteoparticles form under many different phospholipid-reconstitution conditions and are stable in most detergents [24]. We therefore conclude that proteoparticles constitute a common TfR superstructure that might be stabilized by homophilic protein–protein interactions.

The high solubility of TfR proteoparticles in detergent-free aqueous solution indicates that the hydrophobic transmembrane domains of the receptor dimers must be shielded against the solvent by large hydrophilic regions. In accordance with the observed size and shape of proteoparticles (Figure 4a) and of the membrane-inserted receptor dimers (Figure 4c), we therefore propose that the transmembrane domains of about nine TfR dimers form a central hydrophobic core surrounded by two hydrophilic shells, the inner one built by the small cytoplasmic regions and the outer one by the large extracellular regions of the receptor (Figure 4b). For symmetry reasons, however, not all nine receptor dimers can occupy equivalent positions. Moreover, the hydrophobic core must be assumed to be structurally less confined, especially as every proteoparticle accommodates, on average, 30.6 phospholipid molecules [24]. The high stability of proteoparticles and their nonperfect symmetry would also explain the inability to grow high-quality crystals from purified human TfR [21]. One could also reason that the lack of a perfect symmetry facilitates the formation of proteoparticles with a size range of six to twelve receptor dimers, as indicated by the broad mass-distribution curve in Figure 2a.

Molecular dimensions of the human TfR dimer

As the arrowheads in Figure 3 indicate, the TfR has a tendency to integrate into the phospholipid bilayer of vesicles and membrane fragments from both sides. In order to analyze the structure of isolated TfR dimers, we digitized the electron micrographs and aligned the images of suitable membrane sections (Figure 4c). Whereas the large extracellular region (672 residues) of the human TfR is clearly visible, the tenfold-smaller cytoplasmic region (67 residues) is not resolved. We show for the first time that a large globular fraction of the extracellular region of the human TfR is separated from the membrane at a fixed distance, indicating the presence of an invisibly thin molecular stalk, as is outlined in the model in Figure 4d. The dimensions of the membrane-inserted TfR dimer were determined by analyzing 72 digitized receptor images. The visible globular domain of the receptor dimer has an average height (perpendicular to the membrane) of 6.4 ± 0.8 nm and a width (parallel to the membrane) of 9.0 ± 1.5 nm. The molecular

Figure 2

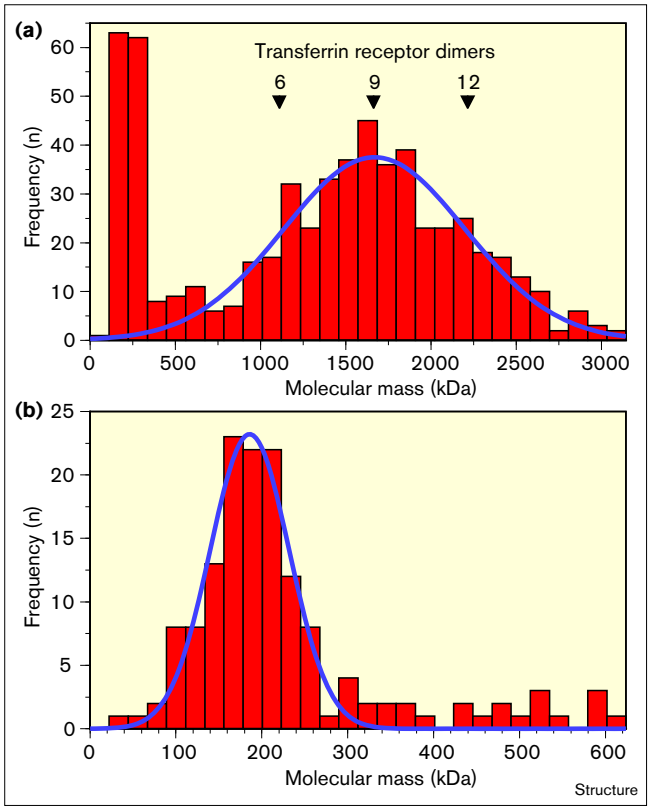

Mass determination of proteoparticles and single TfR dimers by STEM darkfield signal analysis of freeze-dried, unstained preparations. The mass of individual structures was determined as described in the Materials and methods section. **(a)** The mass distribution of all analyzed structures. A Gaussian curve fit of the broad major peak yielded an average mass for the proteoparticles of 1669 ± 26 kDa corresponding to nine TfR dimers. Arrowheads mark the standard deviation of about ± 3 TfR dimers ($\sigma = 533$ kDa). **(b)** The left peak of (a) at a higher-resolution. The average molecular mass of the particles was determined to be 185.9 ± 4.2 kDa and corresponds perfectly to the published mass of the human TfR dimer [11,26–28].

Figure 3

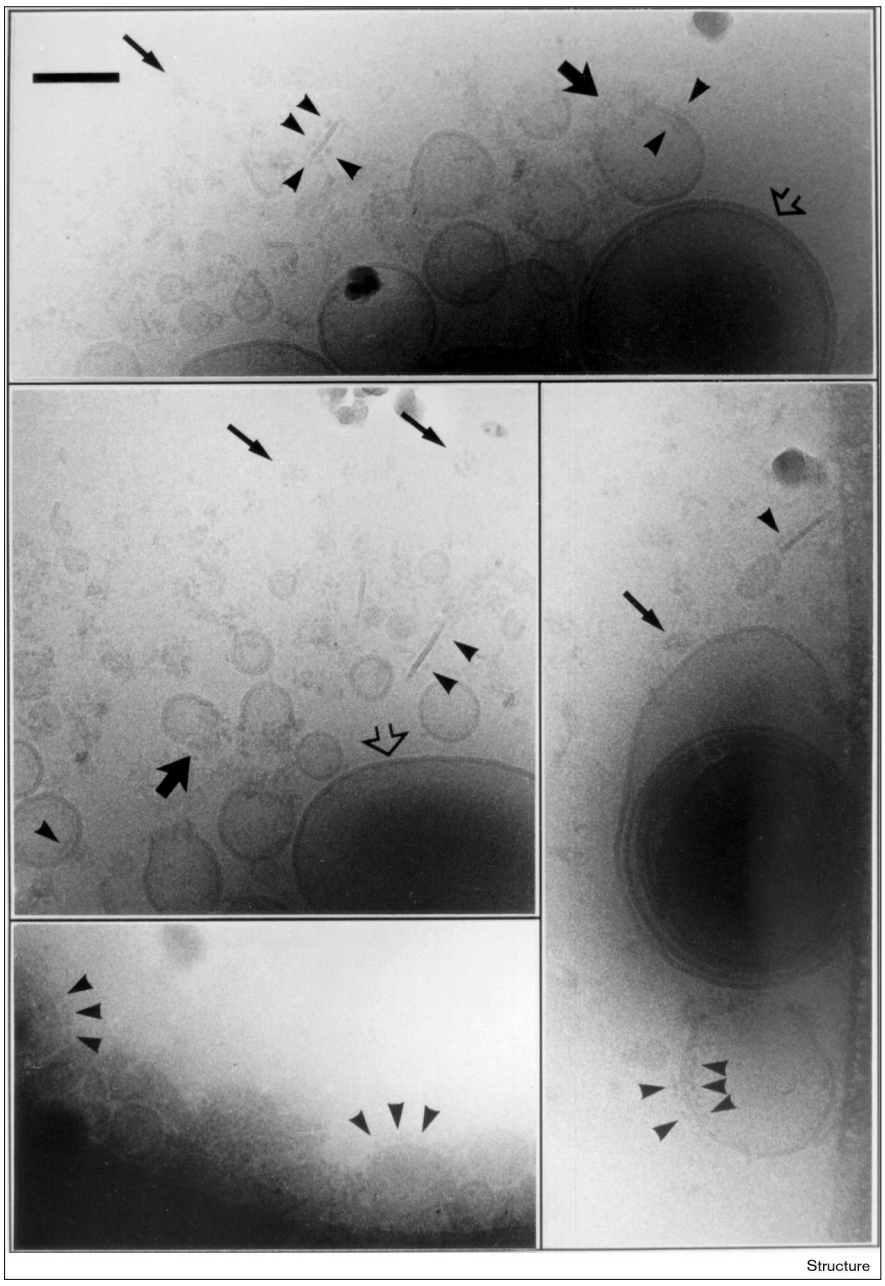

Cryo-EM images of membrane-reconstituted human TfR and single proteoparticles. The 8-POE-solubilized TfR was reconstituted into preformed SBL vesicles by dialysis and imaged in vitreous ice over holes in the carbon support film at 100K. Arrowheads point to the large extracellular domains of reconstituted human TfR. In addition to the membrane-reconstituted receptor molecules, a number of TfR proteoparticles (thin arrows) were found that resembled, in size and shape, those visualized by STEM (Figure 1). Some vesicles are clustered on one side with groups of proteoparticles (thick arrows). A few large unilamellar or multilamellar vesicles are completely receptor-free (open arrows).

stalk linking the globular extracellular domain (gEC) to the transmembrane domain (TM) has a length of 2.9 ± 0.8 nm. The reconstituted phospholipid bilayer is 6.6 ± 0.5 nm thick.

As a result of the membrane insertion, all receptor heads are locked at the same distance from the membrane but are free to rotate about their stalk. Thus, only the height of the globular domain can be determined accurately; the apparent width represents an average of all angular projections. Assuming that all molecular dimensions determined by EM are affected by the same experimental error, the twofold-larger standard deviation of the width ($\sigma = 1.5$ nm) relative to that of the height of the receptor head ($\sigma = 0.8$) indicates that the width varies by about 3 nm depending on the projection angle. An ellipsoid with the respective dimensions of $6.4 \times 7.5 \times 10.5$ nm accommodates 193 kDa of protein with a density of 1.37 g/ml. The ratio between the largest and shortest axes of 1.64 is much smaller than the ratio, deduced by gel filtration, of 3.1 for the large tryptic fragment of the human TfR [31]. This difference may be explained by the limits of the gel filtration method,

Figure 4

Images and models of proteoparticles and membrane-reconstituted human TfR. Cryo-electron-microscopic images of proteoparticles and membrane fragments were digitized and analyzed as described. **(a)** Four typical proteoparticles. **(b)** A proteoparticle model. **(c)** Two typical membrane fragments. **(d)** The corresponding model. Proteoparticles and receptor dimers inserted from opposite sides into the membrane have similar cross-sections of 28.1 nm and 26.2 nm, respectively. Scale bars: 25 nm.

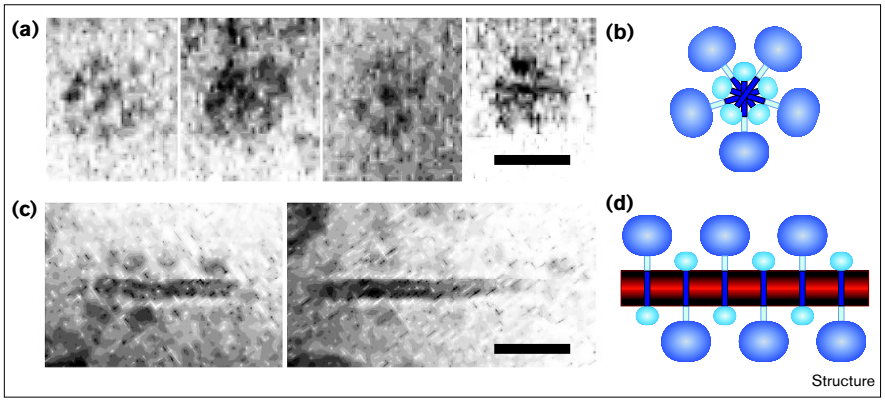

however, because the simultaneously determined axis ratio of 3.4 for human transferrin [31] is also much larger than the factor of 2.0 derived from the crystal structure of human lactoferrin [32], which exhibits 55% amino acid sequence identity with human transferrin [33].

Defining the stalk region of human TfR

A soluble form of the human TfR, the serum transferrin receptor, is released *in vivo* upon proteolytic cleavage [10] at Arg100. The resulting large fragment of the extracellular region (residues 101–760) retains both the homodimerization and the ligand-binding activities [34]. In addition, the purified human TfR is efficiently cleaved by mild tryptic digestion into a small peptide ending at Arg121 and a large globular fragment that elutes from a gel filtration column as a homodimer with an apparent molecular mass of 151 kDa [31]. This even smaller extracellular fragment (residues 122–760) still binds transferrin ([31], HF and RG, unpublished results). As both the serum TfR and the large tryptic fragment lack the two intermolecular disulfide bridges (Cys89 and Cys98) but still remain in the homodimeric state, the ligand-binding site as well as the dimer interface must be completely retained in those large globular fragments. We therefore conclude that the main function of the region preceding the transmembrane domain is the formation of a thin stalk that bridges the gap, seen in the cryo-EM images, between the large globular domain and the phospholipid bilayer. If this is the sole function of the stalk domain, however, its amino acid sequence should have been less conserved during evolution than those of domains involved in highly specific protein–protein interactions, such as the large globular domain. Accordingly, we have compared the protein sequence of human TfR with all three published TfR sequences from other vertebrates: mouse [35,36], hamster [37] and chicken [38]. The result of this analysis is shown in Figure 5, which illustrates the chemical similarity between human and chicken TfRs. Most strikingly, the extracellular region directly following the transmembrane domain (S1, residues 89–126) was found to be the least conserved region of the entire protein. This region contains the two intermolecular disulfide bridges (Cys89 and Cys98) and both proteolytic-cleavage sites (Arg100 and Arg121). Further towards the C terminus, a second

Figure 5

Comparison of the amino acid sequences of human TfR and the TfR from chicken. The cytoplasmic domain (CP), the transmembrane domain (TM), the proposed stalk domains (S1, S2) and the globular extracellular domain (gEC) of human TfR were compared to the respective chicken TfR domains. The domain-specific average chemical sequence similarity is plotted against the amino acid position of human TfR. The dotted line represents the average chemical sequence similarity of the whole protein. The sequence regions that correspond to the major tryptic fragment and to the serum TfR are indicated.

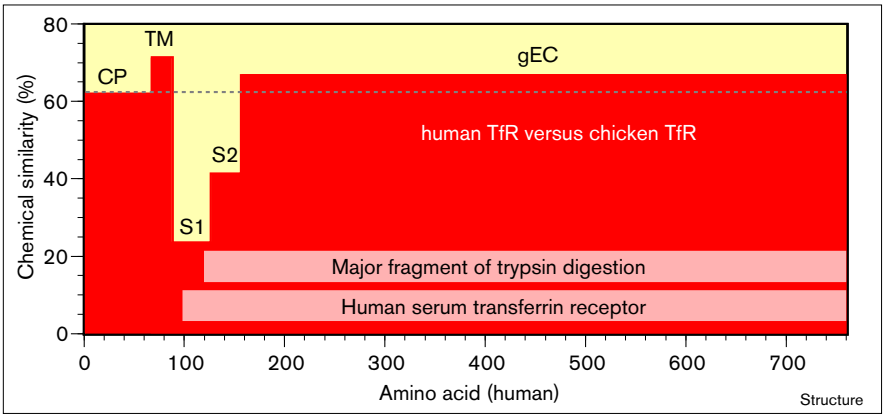

Table 1

Domain-specific sequence comparison of human TfR with TfR from chicken, mouse and hamster.

Domain	hTfR residues	Human to chicken		Human to mouse		Human to hamster	
		Amino acid identity	Chemical similarity	Amino acid identity	Chemical similarity	Amino acid identity	Chemical similarity
Overall identity (%)							
All domains	1–760	49.9	62.8	75.8	84.7	78.5	86.5
Local difference identity							
CP*	1–67	5.0	−0.8	12.3	4.9	5.1	0.1
TM†	68–88	2.4	8.6	−9.1	5.8	7.2	13.5
S1‡	89–126	−34.3	−39.3	−25.8	−29.7	−32.3	−32.6
S2‡	127–155	−25.8	−21.4	−17.1	−12.3	−23.3	−24.4
gEC§	156–760	3.4	4.0	1.5	1.8	2.4	2.8

*Cytoplasmic domain. †Transmembrane domain. ‡Possible spacer segments. §Globular extracellular domain.

domain (S2, residues 127–155) that exhibits an intermediate level of interspecies conservation was identified. We therefore propose that the S1 domain corresponds to the molecular stalk, whereas the S2 domain forms a transition domain between the stalk and the large globular domain. This conclusion is further supported by the fact that similar results were obtained in all possible sequence comparisons, irrespective of whether amino acid identities or chemical similarities were considered (Table 1).

Structural model of the human TfR

As previously described, the TfR consists of a small cytoplasmic region containing an internalization signal, a single transmembrane domain and a large extracellular domain [13,18,19,39]. A combination of cryo-EM analysis and comparative sequence interpretation has now allowed us to derive a low-resolution picture of the organization of the TfR molecule (Figure 6). The proposed model not only accounts for a number of published structural results, but also allows us to explain a number of biochemical observations. The molecular stalk separates the receptor head from the lipid bilayer by 2.9 nm. This stalk region is easily accessible to proteases but appears to be partially protected by the O-glycosylation of Thr104, which interferes with the proteolytic event that produces the serum TfR [40]. The secondary structure of the stalk region is unlikely to be a continuous α helix because four proline residues are located at positions 94, 107, 112 and 117, the last of these being conserved among mammals. The two globular extracellular domains of the TfR dimer contain both the homodimerization site and the transferrin-binding site. They form a well-resolved, large globular domain with a size of $6.4 \times 7.5 \times 10.5$ nm. The stalk is not required for dimer formation and it contains two disulfide bonds that are neither essential for receptor biosynthesis nor for transport of the receptor to the cell surface [14]. As both disulfide bonds are located very close to the membrane, they may rather be important for keeping the transmembrane domains of the receptor dimer attached.

Figure 6

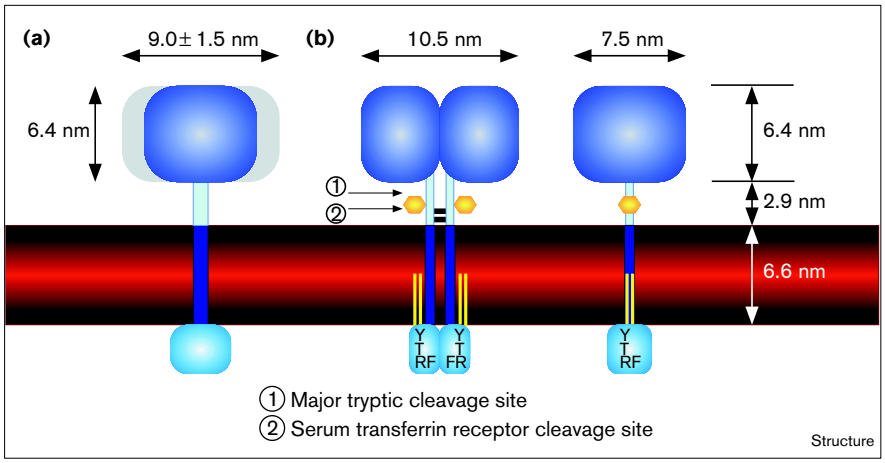

Transferrin receptor model. **(a)** Average dimensions of the receptor dimer derived by EM image analysis. **(b)** Structural model incorporating additional biochemical data (see Results and discussion section). The receptor dimer is shown in two projections that are perpendicular to each other. Several covalent modifications of the receptor referred to in the text are also indicated. Independent data suggest that the disulfide bonds (black bars), the *O*-glycans (yellow hexagons), and the protease cleavage sites (arrows) are part of a molecular stalk that is formed by amino acids 89–126 of the receptor. YTRF (single-letter amino acid code), is the internalization motif of the TfR.

Biological implications

Upon phospholipid reconstitution of the human transferrin receptor (TfR), we have previously observed tubuli and rosette-like structures called proteoparticles [24], in addition to vesicles. In order to understand the structural basis for this unexpected structural heterogeneity of TfR and to draw further biological conclusions, we have now analyzed membrane-inserted and proteoparticle-bound human TfR with electron-microscopic (EM) methods.

In sheep, the TfR is expelled from reticulocytes during maturation in the form of round bodies with 50 nm diameter [41]. Negative-stain EM images of these round bodies resemble, in size and shape, our cryo-EM images of vesicle-associated proteoparticles. The close association of the proteoparticles and the presence of obvious transition states suggest a dynamic transition between proteoparticles and membrane-inserted TfR. This observation and the unusual stability of TfR proteoparticles could therefore reflect an intrinsic self-association potential of TfR being utilized during sheep reticulocyte maturation. Furthermore, recent light-scattering experiments indicate a tendency of the human TfR proteoparticles to form larger clusters upon either deglycosylation or solvent acidification (J Schüler, Y Georgalis, HF, P Umbach, W Saenger & RG, unpublished results). This induced self-association may be linked to the observed separation of TfR from other endocytosed membrane proteins and to its subsequent return to the cell surface within tubular structures.

Upon purifying TfR from different subcellular fractions, Turkewitz and Harrison [42] had previously observed that receptor molecules derived from coated vesicles self-associated into larger aggregates of unspecified size. On the basis of their observations, they had already concluded that the lower pH within coated vesicles could trigger a specific self-association process that might be involved in receptor sorting. Our current findings together with the results of our light-scattering experiments (J Schüler, Y Georgalis, HF, P Umbach, W Saenger & RG, unpublished results) support this hypothesis.

An unexpected finding is the observation that the human TfR seems preferentially to integrate into vesicles with a diameter of between 60 and 160 nm, whereas larger vesicles remain essentially receptor-free. It is interesting to note that this preferred size resembles that of plasma-membrane-derived coated vesicles (100 nm diameter) and endosomal TfR-containing clathrin-coated buds (60 nm) [3]. This selective affinity of the human TfR for vesicles of a certain size further supports the suggestion that the TfR self-association potential is linked to sorting events along its intracellular path.

Our discovery of a molecular spacer of 2.9 nm that keeps the TfR ligand-binding domain at a constant distance from the membrane suggests an important function that might be shared by other endocytic receptors. The 'stalk' increases the motion of the ligand-binding site relative to the membrane. On the one hand, mobility of the ligand-binding site could increase the ligand-association rate and, on the other, it could help to accommodate the receptor–ligand complex in the narrow tubules of the recycling pathway.

Materials and methods

Octyl(polydisperse)oligooxyethylene (8-POE) was obtained from the W. Kolb AG (Hedingen, Switzerland). CHAPS (3-[(3-cholamidopropyl)dimethylammonio]-1-propanesulfonate), soy bean lecithin (SBL) and human transferrin were purchased from Sigma (St. Louis, MO, USA). Human placental transferrin receptor (TfR) was purified by ligand affinity chromatography [31] with the modifications described recently [24].

Reconstitution of TfR in soy bean lecithin vesicles

The TfR (200 μg) was pre-incubated for 30 min in 900 μL of 1.11-fold concentrated TBS (Tris/HCl-buffered saline: 100 mM NaCl, 50 mM Tris(hydroxymethyl)-aminomethane, pH 8.0) containing 1% 8-POE. This detergent had been found to completely solubilize TfR [24]. Preformed SBL vesicles were prepared on ice by sonicating an aqueous suspension of SBL with a Branson Sonifier B-12 (Danbury, Connecticut, USA) for 30 s intervals (intensity setting: 5) until the milky lipid suspension became weakly translucent. Subsequently, the solution was diluted to 20 mg/ml phospholipid. The solubilized protein (900 μl) was mixed with the phospholipid solution (100 μl) and incubated for 1 h at room temperature. Reconstitution was performed at 4°C by dialyzing the sample five times for 3 h against 1 l of TBS. After reconstitution, all samples were centrifuged at 100,000 × g for 2 h at 8°C. The pellets were resuspended in 200 μl TBS and homogenized in a precision Potter homogenizer with a Teflon pestle (Kontes, Vineland, NJ, USA).

Scanning transmission electron microscopy (STEM)

Copper grids (200-mesh) were coated with thick fenestrated carbon films prepared according to the method of Fukami and Adachi [43]. In a second step, the fenestrated carbon films were covered with a thin closed carbon film to yield a thin specimen support. Glow discharge in air was used to enhance protein adsorption. 5 μl TfR solution (85 μg/ml in phosphate-buffered saline – 150 mM NaCl, 10 mM phosphate, pH 7.5) was adsorbed to each grid for 1 min. To remove any salt that could affect the mass determination [44], the grids were washed five times on water droplets and were blotted between each wash step. After washing, the grids were either negatively stained with uranyl formate or blotted, frozen in liquid nitrogen and freeze-dried overnight at −80°C in the pretreatment chamber of the Vacuum Generator's HB-5 scanning transmission electron microscope. The sample was scanned with an electron beam focused to less than 1 nm diameter. The elastic dark-field signal was determined for each raster point by counting the elastically scattered electrons at large angles by an annular detector.

Mass determination of proteoparticles and single TfR dimers

The darkfield counts were stored on a hard disk and used for mass determination by a specialized software package (IMPSYS) as described previously [44,45]. To this end, the circumference of proteoparticles and TfR dimers were contoured at a given threshold intensity, the signal integrated, the background subtracted and the resulting value normalized to the recording dose [44]. Mass values thus obtained were displayed in histograms to which Gaussian profiles could be fitted.

Cryo-electron microscopy

Grids with uncovered thick fenestrated carbon films were prepared as described above and mounted in a shock-freeze chamber adjusted to

25°C and 90% relative humidity. SBL-reconstituted TfR (5 μl) was applied to the grid inside the chamber and incubated for 1 min. After removing excess buffer by paper blotting, the remaining aqueous solution spanning the holes of the carbon film was shock frozen to amorphous ice by dropping the whole grid holder into liquid ethane kept at 90K. All subsequent steps were performed well below 120K, within a nitrogen atmosphere. If required, sample grids were stored in liquid nitrogen. For cryo-EM, the grids were transferred into an electron microscope 902 Cryo (Zeiss, Oberkochen, Germany) and analyzed at 100K. Focusing was performed at a 140,000-fold magnification using the minimal-dose focusing system to avoid beam damage to the frozen sample. Cryo-EM images were recorded at 50,000-fold magnification by exposing a high-resolution film (SO-163, Kodak) for a maximum of 1 s.

Image analysis

Threefold magnified prints of cryo-EM images were scanned at 600 dpi and digitized on an eight-bit grayscale (Agfa-Gaevert StudioScan II). Images of single proteoparticles and membrane fragments were, if necessary, contrast enhanced and aligned. Size determination of the structures was performed by measuring a large number of images and averaging the obtained distances. The overall diameter of proteoparticles was determined by fitting circles or ellipses to 62 different proteoparticles. Ellipses were used sometimes because proteoparticles are not perfectly regular in their shape. Indeed, the measurement revealed an average deviation from a circular shape of 2.4 nm or 7.6%. The thickness of the membrane, the diameter of the globular domain and the length of the TfR stalk were derived from 72 clearly visible molecules integrated in aligned membrane fragments.

Amino acid sequence analysis

Amino acid sequences were derived from the EMBL/GenBank/DDBJ Databases. The protein sequence of human TfR was aligned to those of chicken [38], mouse[35,36], and hamster [37] using the MacMolly Tetra software package (version 2.1, Soft Gene GmbH, Berlin, Germany). The similarity of the three major parts of the protein – the cytoplasmic region, the transmembrane domain and the extracellular region – was quantified by calculating the respective amino acid identity and the chemical similarity according to the definitions of Kruskal [46].

Acknowledgements

We thank M Swoboda for the generous help in producing the cryo-EM images and KN Goldie for performing the STEM images of proteoparticles. The STEM work was supported by the Swiss National Fund for Research and the Maurice Müller foundation of Switzerland. HF received a graduate scholarship (NaFöG) and a DAAD foreign exchange fellowship.

References

1. Dautry-Varsat, A., Ciechanover, A. & Lodish, H.F. (1983). pH and the recycling of transferrin during receptor-mediated endocytosis. *Proc. Natl Acad. Sci. USA* **80**, 2258-2262.
2. Hopkins, C.R., Gibson, A., Shipman, M., Strickland, D.K. & Trowbridge, I.S. (1994). In migrating fibroblasts, recycling receptors are concentrated in narrow tubules in the pericentriolar area, and then routed to the plasma membrane of the leading lamella. *J. Cell Biol.* **125**, 1265-1274.
3. Stoorvogel, W., Oorschot, V. & Geuze, H.J. (1996). A novel class of clathrin-coated vesicles budding from endosomes. *J. Cell Biol.* **132**, 21-33.
4. Harford, J.B. & Klausner, R.D. (1990). Coordinate post-transcriptional regulation of ferritin and transferrin receptor expression: the role of regulated RNA-protein interaction. *Enzyme* **44**, 28-41.
5. Theil, E.C. (1990). Regulation of ferritin and transferrin receptor mRNAs. *J. Biol. Chem.* **265**, 4771-4774.
6. Ward, J.H., Kushner, J.P. & Kaplan, J. (1982). Regulation of HeLa cell transferrin receptors. *J. Biol. Chem.* **257**, 10317-10323.
7. Snider, M.D. & Rogers, O.C. (1985). Intracellular movement of cell surface receptors after endocytosis: resialylation of asialo-transferrin receptor in human erythroleukemia cells. *J. Cell Biol.* **100**, 826-834.
8. Enns, C.A., Mulkins, M.A., Sussman, H. & Root, B. (1988). Modulation of the transferrin receptor during DMSO-induced differentiation in HL-60 cells. *Exp. Cell Res.* **174**, 89-97.
9. Pan, B.T. & Johnstone, R.M. (1983). Fate of the transferrin receptor during maturation of sheep reticulocytes in vitro: selective externalization of the receptor. *Cell* **33**, 967-978.
10. Shih, Y.J., Baynes, R.D., Hudson, B.G., Flowers, C.H., Skikne, B.S. & Cook, J.D. (1990). Serum transferrin receptor is a truncated form of tissue receptor. *J. Biol. Chem.* **265**, 19077-19081.
11. Omary, M.B. & Trowbridge, I.S. (1981). Covalent binding of fatty acid to the transferrin receptor in cultured human cells. *J. Biol. Chem.* **256**, 4715-4718.
12. Davis, R.J., Johnson, G.L., Kelleher, D.J., Anderson, J.K., Mole, J.E. & Czech, M.P. (1986). Identification of serine-24 as the unique site on the transferrin receptor phosphorylated by protein kinase C. *J. Biol. Chem.* **261**, 9034-9041.
13. Alvarez, E., Gironès, N. & Davis, R.J. (1990). Inhibition of the receptor-mediated endocytosis of diferric transferrin is associated with the covalent modification of the transferrin receptor with palmitic acid. *J. Biol. Chem.* **265**, 16644-16655.
14. Jing, S.Q. & Trowbridge, I.S. (1987). Identification of the intermolecular disulfide bonds of the human transferrin receptor and its lipid-attachment site. *EMBO J.* **6**, 327-331.
15. Do, S.I. & Cummings, R.D. (1992). Presence of O-linked oligosaccharide on a threonine residue in the human transferrin receptor. *Glycobiology* **2**, 345-353.
16. Hayes, G.R., Enns, C.A. & Lucas, J.J. (1992). Identification of the O-linked glycosylation site of the human transferrin receptor. *Glycobiology* **2**, 355-359.
17. Orberger, G., Geyer, R., Stirm, S. & Tauber, R. (1992). Structure of the N-linked oligosaccharides of the human transferrin receptor. *Eur. J. Biochem.* **205**, 257-267.
18. McClelland, A., Kuhn, L.C. & Ruddle, F.H. (1984). The human transferrin receptor gene: genomic organization, and the complete primary structure of the receptor deduced from a cDNA sequence. *Cell* **39**, 267-274.
19. Schneider, C., Owen, M.J., Banville, D. & Williams, J.G. (1984). Primary structure of human transferrin receptor deduced from the mRNA sequence. *Nature* **311**, 675-678.
20. Maxfield, F.R. & Yamashiro, D.J. (1991). In *Intracellular Trafficking of Proteins*. (Steer, C.J. & Haanover, J.A., eds), pp. 157-182, Cambridge University Press, New York.
21. Borhani, D.W. & Harrison, S.C. (1991). Crystallization and X-ray diffraction studies of a soluble form of the human transferrin receptor. *J. Mol. Biol.* **218**, 685-689.
22. Kurrle, A., Rieber, P. & Sackmann, E. (1990). Reconstitution of transferrin receptor in mixed lipid vesicles. An example of the role of elastic and electrostatic forces for protein/lipid assembly. *Biochemistry* **29**, 8274-8282.
23. Demant, E.J., Christiansen, K. & Tranum, J.J. (1992). The human placental transferrin receptor: reconstitution into liposomes and electron microscopy. *Biosci. Rep.* **12**, 471-482.
24. Fuchs, H., Geßner, R., Tauber, R. & Ghosh, R. (1995). Functional reconstitution of the human placental transferrin receptor into phospholipid bilayers leads to long tubular structures proceeding from the vesicle surface. *Biochemistry* **34**, 6196-6207.
25. Engel, A. (1978). Molecular weight determination by scanning transmission electron microscopy. *Ultramicroscopy* **3**, 273-281.
26. Seligman, P.A., Schleicher, R.B. & Allen, R.H. (1979). Isolation and characterization of the transferrin receptor from human placenta. *J. Biol. Chem.* **254**, 9943-9946.
27. Enns, C.A. & Sussman, H.H. (1981). Physical characterization of the transferrin receptor in human placentae. *J. Biol. Chem.* **256**, 9820-9823.
28. Hunt, R.C., Riegler, R. & Davis, A.A. (1989). Changes in glycosylation alter the affinity of the human transferrin receptor for its ligand. *J. Biol. Chem.* **264**, 9643-9648.
29. Boekema, E.J. & Lücken, U. (1996). The structure of the CF^1 part of the ATP-synthase complex from chloroplasts. In *Oxygenic photosynthesis: The light reactions*. (Ort, D.R. & Yocum, C.F., eds), pp. 487-492, Kluwer Academic Publishers, Netherlands.
30. Gogol, E.P., Lücken, U. & Capaldi, R.A. (1987). The stalk connecting the F^1 and F^0 domains of ATP-synthase visualized by electron microscopy of unstained specimens. *FEBS Lett.* **219**, 274-278
31. Turkewitz, A.P., Amatruda, J.F., Borhani, D., Harrison, S.C. & Schwartz, A.L. (1988). A high yield purification of the human transferrin receptor and properties of its major extracellular fragment. *J. Biol. Chem.* **263**, 8318-8325.
32. Anderson, B.F., *et al.*, & Baker, E.N. (1987). Structure of human lactoferrin at 3.2-resolution. *Proc. Natl Acad. Sci. USA* **84**, 1769-1773.

33. Yang, F., *et al.*, & Bowman, B.H. (1984). Human transferrin: cDNA characterization and chromosomal localization. *Proc. Natl Acad. Sci. USA* **81**, 2752-2756.
34. Huebers, H.A., Beguin, Y., Pootrakul, P., Einspahr, D. & Finch, C.A. (1990). Intact transferrin receptors in human plasma and their relation to erythropoiesis. *Blood* **75**, 102-107.
35. Stearne, P.A., Pietersz, G.A. & Goding, J.W. (1985). cDNA cloning of the murine transferrin receptor: sequence of trans-membrane and adjacent regions. *J. Immunol.* **134**, 3474-3479.
36. Trowbridge, I.S., Domingo, D.L., Thomas, M.L. & Chain, A. (1991). In *Mus Musculus mRNA for transferrin receptor*, EMBL/GenBank/DDBJ Databases [accession number X57349].
37. Collawn, J.F., Lai, A., Domingo, D., Fitch, M., Hatton, S. & Trowbridge, I.S. (1993). YTRF is the conserved internalization signal of the transferrin receptor, and a second YTRF signal at position 31-34 enhances endocytosis. *J. Biol. Chem.* **268**, 21686-21692.
38. Gerhardt, E.M., Chan, L.N., Jing, S.Q., Qi, M.Y. & Trowbridge, I.S. (1991). The cDNA sequence and primary structure of the chicken transferrin receptor. *Gene* **102**, 249-254.
39. Collawn, J.F., *et al.*, & Tainer, J.A. (1990). Transferrin receptor internalization sequence YXRF implicates a tight turn as the structural recognition motif for endocytosis. *Cell* **63**, 1061-1072.
40. Rutledge, E.A., Root, B.J., Lucas, J.J. & Enns, C.A. (1994). Elimination of the O-linked glycosylation site at Thr-104 results in the generation of a soluble human-transferrin receptor. *Blood* **83**, 580-586.
41. Johnstone, R.M., Mathew, A., Mason, A.B. & Teng, K. (1991). Exosome formation during maturation of mammalian and avian reticulocytes: evidence that exosome release is a major route for externalization of obsolete membrane proteins. *J. Cell Physiol.* **147**, 27-36.
42. Turkewitz, A.P. & Harrison, S.C. (1989). Concentration of transferrin receptor in human placental coated vesicles. *J. Cell Biol.* **108**, 2127-2135.
43. Fukami, A. & Adachi, K. (1965). A new method of preparation of a self-perforated micro plastic grid and its application. *J. Electron Microsc.* **14**, 112.
44. Müller, S.A., Goldie, K.N., Bürki, R., Häring, R. & Engel, A. (1992). Factors influencing the precision of quantitative scanning transmission electron microscopy. *Ultramicroscopy* **46**, 317-334.
45. Engel, A. & Reichelt, R. (1988). Processing of quantitative scanning transmission electron micrographs. *Scanning Microsc.* Suppl. **2**, 285-293.
46. Kruskal, J.B. (1983). The theory and practice of sequence comparison. In*Time warps, string edits, and macromolecules.* (Sankoff, D. & Kruskal, J.B., eds), pp. 1-44, Addison-Wesley Publ. Comp., Inc., London.